Highly efficient activation of HCl dissociation on Au(111) via rotational preexcitation

Gerrits, N.; Geweke, J.: Auerbach, D.; Beck, R.D.; Kroes, G.J.

Note: To cite this publication please use the final published version (if applicable).

Letter

Highly Efficient Activation of HCl Dissociation on Au(111) via Rotational Preexcitation

Nick Gerrits,* Jan Geweke, Daniel J. Auerbach, Rainer D. Beck, and Geert-Jan Kroes*

Cite This: *J. Phys. Chem. Lett.* 2021, 12, 7252−7260

Read Online

ACCESS | Metrics & More | Article Recommendations | Supporting Information

ABSTRACT: The probability for dissociation of molecules on metal surfaces, which often controls the rate of industrially important catalytic processes, can depend strongly on how energy is partitioned in the incident molecule. There are many example systems where the addition of vibrational energy promotes reaction more effectively than the addition of translational energy, but for rotational pre-excitation similar examples have not yet been discovered. Here, we make an experimentally testable theoretical prediction that adding energy to the rotation of HCl can promote its dissociation on Au(111) 20 times more effectively than increasing its translational energy. In the underlying mechanism, the molecule's initial rotational motion allows it to pass through a critical region of the reaction path, where this path shows a strong and nonmonotonic dependence on the molecular orientation.
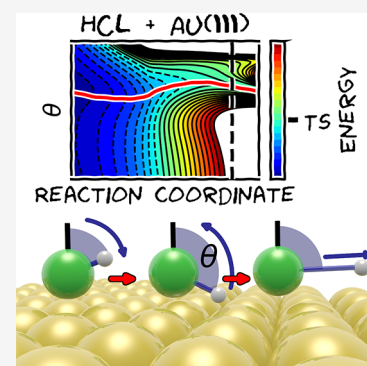
Fundamental understanding of molecule−metal surface reaction (MMSR) mechanisms is vital for understanding industrial catalysis as the rates of MMSRs may determine the rates of industrial processes.[1−5] The rate of an industrial heterogeneously catalyzed process, which consists of a sequence of elementary surface reactions, is often controlled[6] by the transition state (TS) of a dissociative chemisorption reaction on a metal surface,[6−8] as is the case in ammonia production[2] and steam reforming.[3] Passage over the transition state may depend not only on the total energy available but also on more subtle dynamical features like the form of the available incidence energy.[9−28] For instance, many,[29−31] although not all, dissociative chemisorption reactions[32] display reaction probabilities that depend only on the fraction of the molecule's translational energy that is associated with motion normal to the surface (normal energy scaling, NES). Another example is that putting additional vibrational energy in an incident molecule usually increases its reaction probability, with an efficacy that differs from that achieved by enhancing its incident translational energy by the same amount.[9−14,17,18,33−35] For some systems, increasing the vibrational energy is even more effective at increasing the reaction probability than increasing the translational energy, in which case we say that the vibrational efficacy exceeds one.[10,17,21,22,25,34,35]

In contrast, increasing the rotational energy of a molecule incident on a metal surface is usually not very effective at increasing the reaction probability. To the best of our knowledge, the rotational efficacy has always been found to be lower than one; that is, adding rotational energy is less effective at promoting reaction than adding the same amount of translational energy. For example, in the benchmark MMSR of H_2 + Cu(111) rotational energy only has a small influence on the dissociation probability[30,31,36,37] (the rotational efficacy is 0.30.5[30,31]), and a similar effect has been observed for H_2 on other metal surfaces.[38−42] In the mechanism found to be operative for H_2 reacting on coinage metal surfaces, rotational energy is converted to energy in motion along the reaction path because the rotational constant of the molecule decreases as its bond length extends upon approaching the late barrier.[30,31] Adding rotational energy has an even smaller effect on the dissociative chemisorption of methane on Ni(111).[43]

We now turn to an examination of the dissociative chemisorption reaction of HCl on Au(111) and the prediction that there can be much stronger effects of rotational motion. We were drawn to this reaction because it has been called an enigmatic reaction.[44] The first measured sticking probabilities (S_0)[45] were found to be 2 orders of magnitude lower than previously predicted values,[46] and the analysis of the experiments suggested a very high vibrational efficacy (see also section S3). Subsequent dynamics calculations managed to reduce the discrepancies between computed and measured S_0 values, but the computed S_0 still exceeded the measured values by 1 order of magnitude.[44,47,48] More recently, considerably better agreement between theory and experiment
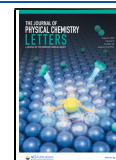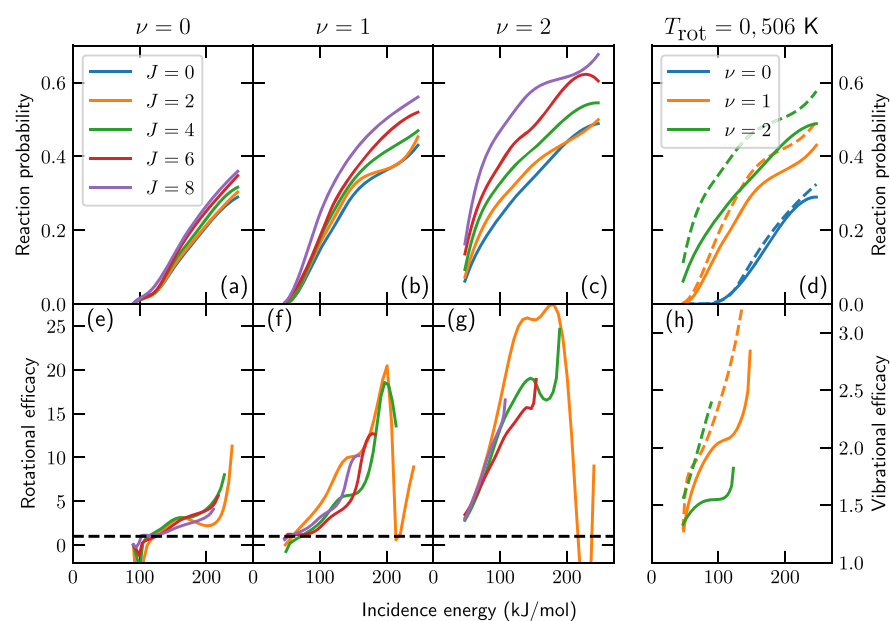
Figure 1. (a−c) Reaction probabilities for normally incident HCl on Au(111) and (e−g) the corresponding rotational efficacy. Results for $\nu = 0$ are shown in panels a and e, for $\nu = 1$ in panels b and f, and for $\nu = 2$ in panels c and g. The rotational efficacy is computed relative to $J = 0$ with the same vibrational state. The dashed line indicates a rotational efficacy of unity. (d) Reaction probability and (h) concomitant vibrational efficacy. The vibrational efficacy is computed relative to $\nu = 0$ with the same rotational state distribution. The solid (dashed) lines indicate results for $T_{rot} = 0$ K (506 K).

Table 1. Rotational (χ_J) and Vibrational (χ_ν) Efficacies of HCl on Au(111) as a Function of the Reaction Probability (Eq 1)^a

	$\chi_{J=2}$			$\chi_{J=4}$			$\chi_{J=6}$			$\chi_{J=8}$			$\chi_\nu(J=0)$		$\chi_\nu(T_{rot}=506\text{ K})$	
R	$\nu=0$	1	2	0	1	2	0	1	2	0	1	2	$0\to1$	$0\to2$	$0\to1$	$0\to2$
0.05	0.5	2.0		1.0	0.8		0.6	1.2		1.1	1.2		1.7		1.8	
0.10	2.2	3.8	5.3	2.2	1.8	3.1	1.4	1.2		1.2	1.6		1.9	1.4	2.0	
0.15	3.1	6.5	10.9	3.1	3.1	6.0	2.6	1.6	4.0	1.9	2.2		2.0	1.5	2.2	1.7
0.20	2.3	9.8	18.7	3.4	5.0	9.9	3.4	2.8	6.0	2.4	3.1	4.1	2.1	1.5	2.4	1.9
0.25	2.9	10.4	25.3	4.7	5.7	13.9	4.0	3.7	8.4	3.0	3.8	5.9	2.2	1.6	2.7	2.1
0.30		14.6	25.7		6.6	16.6		4.6	10.8		4.5	7.9			3.1	2.3
0.35		19.1	27.5		12.3	18.8		7.7	13.0		6.8	10.1				
0.40		3.9	20.2		18.3	17.7		12.5	14.6		9.9	11.9				
max	5.4	8.9	11.4	10.8	13.6	24.6	6.9	12.6	18.9	17.6	10.2	16.6	2.8	1.8	3.3	2.4

^{a}In the column where R is given as "max" the rotational or vibrational efficacy is presented for the maximum value of the reaction probability for which it could be evaluated.

was achieved for sticking at normal incidence.[25] The improved agreement resulted from the theory using a better density functional (DF, the MS-RPBEl meta-generalized gradient approximation (meta-GGA) functional[49]) and a reanalysis of the experiments concerning, for instance, the relationship between the sticking probability and the Auger signals used to establish the coverage of Au by Cl.[25] As a result, the discrepancy between the computed and measured sticking probabilities at normal incidence was reduced to a factor ranging from 2 to 7, depending on the incidence energy. The remaining discrepancy between theory and experiment is expected to be due to the DF[50] since previous work for HCl + Au(111) has shown that the dynamics and PES fitting methods employed, and the neglect of electron−hole pair excitation, do not affect the sticking or (in)elastic scattering probability considerably[44,47,48,51] (see also section S2). Nevertheless, the trends observed experimentally in the energy transfer[52] and (in)elastic scattering probabilities[53] were reproduced qualitatively, suggesting that the new potential energy surface (PES) should be adequate for describing the reaction

mechanism of HCl + Au(111). However, sticking at off-normal incidence and the unusually large vibrational efficacy implicit in a former analysis of the experiments[45] were not yet addressed.

Here, we also consider the sticking of HCl on Au(111) at off-normal incidence, paying special attention to the effects of the rotational temperature of the incident molecular beam and its average incidence energy parallel to the surface (see also section S5). For this, the previous experiments on sticking at off-normal incidence were reanalyzed in the same way as done before for normal incidence.[25] Also, the same improved PES was used as in our previous successful study of scattering at normal incidence.[25] The theory yields an even better description of sticking at off-normal incidence than previously obtained for normal incidence.[25]

To our complete surprise, the calculations showed very high rotational efficacies for reaction, with values exceeding 10. This high rotational efficacy is caused by a strong and non-monotonic dependence of the reaction path on the polar angle θ of the orientation of HCl relative to the Au(111) surface in a

region of this path that just precedes the barrier. To traverse this region and encounter a relatively low barrier to dissociation, the molecule needs to rotate initially, and it needs to arrive at this region with the right rotational phase. Furthermore, the predicted rotational efficacy is strongly dependent on the employed DF. For instance, GGA DFs predict a very low rotational efficacy instead, making the predicted rotational efficacy an important fingerprint of the accuracy of a DF for HCl + Au(111) relative to experiment (see section S7 for additional details).

To explore the large rotational efficacy, we first consider normally incident HCl. Figures 1a−c show the initial state selected reaction probability $R_{\nu,J}(E_i)$, where ν is the initial vibrational and J the initial rotational quantum number. There is a large dependence of $R_{\nu,J}(E_i)$ on J for $\nu = 0, 1$, and especially 2. We define the rotational efficacy, which measures how effective adding rotational energy is at promoting the reaction (i.e., at achieving an initial state-selected reaction probability equal to R) relative to increasing E_i for HCl in the state ν, as follows:

$$\chi_J(R; \nu) = \frac{E_i(\nu, J = 0; R) - E_i(\nu, J; R)}{E_{rot}(\nu, J) - E_{rot}(\nu, J = 0)} \quad (1)$$

Here, $E_i(\nu,J;R)$ is the incidence energy at which $R_{\nu,J}(E_i) = R$.

Table 1 shows that rotational efficacies defined in this way may be large; for example, for $J = 6$ it takes on the values of 6.9 for $\nu = 0$, of 12.6 for $\nu = 1$, and of 18.9 for $\nu = 2$. In writing and applying eq 1, we have tentatively assumed that $R_{\nu,J}(E_i)$ is a bijective or invertible function; that is, only one value of E_i corresponds to a particular value of $R_{\nu,J}$. This will usually be true as $R_{\nu,J}(E_i)$ tends to be a monotonically increasing function of E_i. We may then also define a function $E_i^{\nu,J}(R)$, which is equal to the incidence energy E_i at which $R_{\nu,J}(E_i) = R$. This allows us to define a rotational efficacy that depends on incidence energy for the molecule in the state ν as follows:

$$\chi_J(E_i; \nu) = \frac{E_i(\nu, J = 0; R) - E_i(\nu, J; R)}{E_{rot}(\nu, J) - E_{rot}(\nu, J = 0)} \quad (2)$$

In eq 2, the argument of χ_J, E_i, is the incidence energy $E_i(\nu,J;R)$ for which a reaction probability R is obtained for the higher rotational state. The rotational efficacy defined in this way is plotted in Figures 1e−g. The plots show that the rotational efficacy strongly depends on the value of E_i at which it is evaluated for the higher rotational state, and it also strongly depends on the value of ν.

Figure 1d also shows a large dependence of $R_{\nu,J}(E_i)$ on ν for $J = 0$. To determine the effectiveness of vibrational pre-excitation for promoting reaction, the vibrational efficacies $\chi_\nu(R;J)$ and $\chi_\nu(E_i;J)$ may be defined in a way that is entirely analogous to eqs 1 and 2, respectively. As can be seen from Table 1, $\chi_\nu(R;J)$ can also take on large values (for $J = 0$, these values are up to 2.8 for $\nu = 1$ and up to 1.8 for $\nu = 2$), which are considerably larger than one. However, they are much smaller than the values achieved for $\chi_J(R;\nu)$ (e.g., up to 18.9 for $\nu = 2, J = 6$). Thus, per unit of energy added by pre-excitation, rotational pre-excitation of the molecules present in a molecular beam has a greater effect on the sticking probability $S_0(E_i,T_N,\Theta_i)$ than vibrational pre-excitation. A similar picture emerges from the plots of $\chi_\nu(E_i;J)$, which takes on values of up to 3.3 for $\nu = 1$ and up to 2.4 for $\nu = 2$ (Figure 1h), while $\chi_{J=6}(E_i, \nu = 2)$ takes on values up to 18.9.

Vibrational efficacies may also be evaluated for a thermal rotational distribution instead of for $J = 0$ only. In Figure 1h, we show $\chi_\nu(E_i; T_{rot} = 506 \text{ K})$ for the highest rotational temperature (T_{rot}) achieved in the recent molecular beam experiments on HCl + Au(111). Here, we see a synergistic effect; that is, the effects of increased vibrational and rotational pre-excitation are mutually reinforcing, where the two effects combined yield a larger increase in reaction than the two effects considered separately. To the best of our knowledge, this mutually reinforcing effect has not been observed or predicted before. This synergistic effect might be of great interest to plasma catalysis, where high rotational and vibrational temperatures can play an important role due to the degrees of freedom (DOFs) within the plasma (e.g., translational, electronic, rotational, and vibrational DOFs) not being in thermal equilibrium.[54−56] Present treatments of this topic tend to ignore the effect of rotational states in plasma catalysis on the reactivity of molecules on metal surfaces,[57−61] at most including T_{rot} in the calculation of the entropy. We intend to explore this topic, and the synergism between rotational and vibrational pre-excitation in promoting reactivity, in future work.

Our prediction of a high rotational efficacy will of course be most useful if it can be confirmed with experiments within the present state-of-the-art. In Figure 2, we show that it should be possible to do so. To enable excitation to high J, the
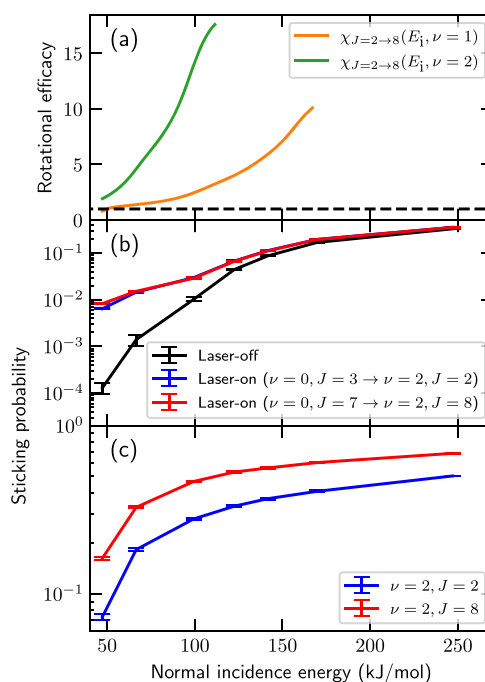
Figure 2. (a) Predicted rotational efficacy of off-normally incident HCl on Au(111) as a function of normal incidence energy. The $J = 2 \rightarrow 8$ rotational efficacy $\chi_{J=2\rightarrow8}(E_i,\nu)$ is determined for $\nu = 1$ (orange) and $\nu = 2$ (green). The dashed line indicates a rotational efficacy of unity. (b) Sticking probability of off-normally incident HCl on Au(111) as a function of normal incidence energy. The black lines indicate "laser-off" results for $T_{vib} = 1060$ K and $T_{rot} = 506$ K. "Laser-on" results, where part of the molecules in the $\nu = 0, J = 3$ ($\nu = 0, J = 7$) state are excited to the $\nu = 2, J = 2$ ($\nu = 2, J = 8$) state, are indicated by the blue (red) lines. (c) State-specific sticking probabilities for the $\nu = 2, J = 2$ (blue) and $\nu = 2, J = 8$ (red) excited states. The error bars represent 68% confidence intervals.
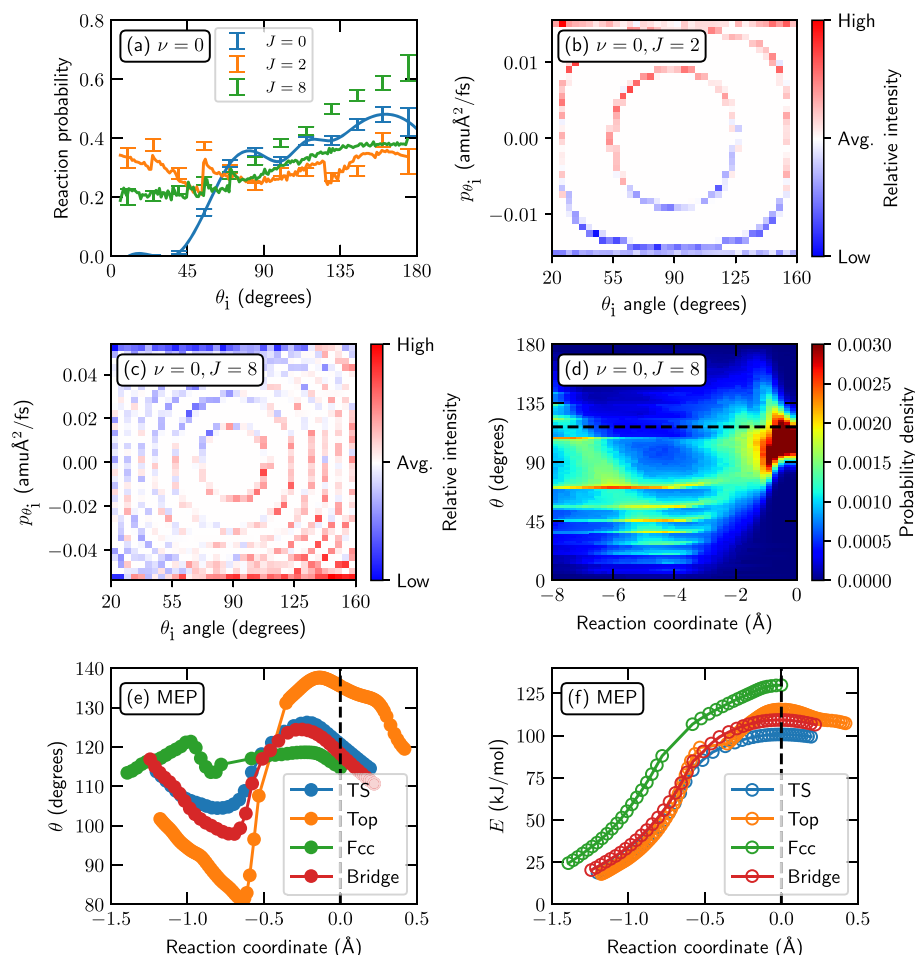
Figure 3. (a) Sticking probability as a function of the initial θ angle of $\nu = 0$ HCl on Au(111) for $\langle E_i \rangle = 247$ kJ/mol for several rotational states as indicated. Results are shown for both an approximate model that neglects angular momentum but takes into account the rotational orientation of HCl (solid line, see section S6 for meaning) and MD simulation (error bars, representing 68% confidence intervals). (b) Distribution of the initial θ angle and its conjugate momentum of reacting HCl on Au(111) for $\nu = 0$ and $J = 2$. The colors indicate the intensity of reactive combinations of θ and p_θ relative to the statistical distribution in the simulated molecular beam; that is, blue indicates that the combination is less reactive compared to its statistical occurrence whereas red indicates a relatively higher reactivity. The data have been normalized along the θ angle to remove the $\sin(\theta)$ distribution in the initial statistical distribution; that is, with the renormalization performed all initial θ angles have equal probability in the statistical distribution. (c) Same as panel b, but showing results for $\nu = 0$ and $J = 8$. (d) Distribution of the θ angle of reacting HCl on Au(111) for $\nu = 0$, $J = 8$, and $E_i = 247$ kJ/mol along the reaction coordinate. The black dashed line indicates the minimum TS value. See ref 25 for the description of the TS. (e) Polar angle θ of HCl on Au(111) along the MEP of the global TS (blue) and the top (orange), hollow (green), and bridge (red) sites. The black dashed line indicates the TS; that is, the value of the reaction coordinate is zero. (f) Same as panel e, but showing the potential energy instead of θ.

experiments we suggest would employ a high nozzle temperature (T_N) and off-normal incidence to vary the normal incidence energy, as done before in the off-normal incidence experiments on HCl + Au(111).[45] Furthermore, we suggest excitation of the incident HCl to the $J' = 2$ and $J' = 8$ states in $\nu' = 1$ or $\nu' = 2$ and direct verification that the reaction of $J = 8$ HCl is far more probable than that of $J = 2$ HCl at similar incidence energy (for additional details, see section S4). Specifically, such an experiment could pre-excite HCl to a specific rovibrational state (here, from $\nu = 0$ and $J = 3$ (one of the highest populated states in the beam previously used with $T_N = 1060$ K and $T_{rot} = 506$ K; see also Figure S2) to $\nu = 1$ or 2 and $J = 2$ or from $\nu = 0$ and $J = 7$ to $\nu = 1, 2$ and $J = 8$) with a laser. Then, from the "laser-off" and "laser-on" results, a state-specific sticking probability could be obtained. Note that in Figure 2b we have accounted for the excitation efficiency in such an experiment. Our calculations strongly suggest that the differences between the laser-off and laser-on results are

measurable for energies below and somewhat above the barrier height, as shown in Figure 2b. The results for $\nu = 1$ are similar (see Figure S3b). For incidence energies far above the barrier height, the differences between the laser-on and laser-off results are small and likely difficult to measure. Note that even though the laser-on sticking probabilities are nearly the same for $J = 2$ and $J = 8$, the state specific reaction probabilities are different because they involve multiplication of the (laser-on−laser-off) sticking probabilities by different factors (see also section S4).

We now turn to the cause of the high rotational efficacy. Our explanation is based on the following remarkable observations. First, as shown in Figure 3a, for $E_i = 247$ kJ/mol $R_{\nu,J}(\theta_i)$ is nonzero for all initial values of the polar orientation angle of HCl for all J-values except for $J = 0$. (Note that $\theta = 0°$ corresponds to the H atom pointing to the gas phase and $\theta = 180°$ to the H atom pointing to the surface; see also Figure S11.) Similar results are obtained for $\nu = 1$ and $\nu = 2$ (see Figure S7). This already suggests a partial explanation for the

high rotational efficacy: Reaction of molecules with high J is comparatively efficient because reaction of $J = 0$ HCl is inefficient. Similarly, vibrational efficacies >1 have previously only been observed if the reaction of a molecule in $\nu = 0$ is inefficient, as found in cases where the reaction of molecules in the vibrational ground state is hampered by the ineffectiveness of translational energy at enabling the system to "turn the corner" in the PES and overcome an energetic barrier late in the reaction coordinate (i.e., the bobsled effect).[10,22] Furthermore, independent of the vibrational state, whether or not a molecule sticks depends not only on the initial value of θ_i but also on its initial conjugate momentum p_θ (see Figures 3b,c). The reason is that the molecule has to arrive at the surface with the right rotational orientation and concomitant motion to access a comparatively low barrier (Figure 3d). Another intriguing observation relevant to the high rotational efficacy is that an approximate model that only takes into account the rotational orientation with which the molecule would arrive at the surface, but excludes the rotational motion prior to reaching the TS (see section S6 for additional details), can reproduce the computed initial distribution of the polar angle θ_i of the reacting molecules reasonably well (Figure 3a). Especially for low J values the agreement between $R(\theta_i,\nu,J)$ yielded by the MD simulations and the approximate model is excellent, although $R(\theta_i, \nu, J)$ is severely underestimated by the approximate model for specific θ_i values for high J, as the promoting effect of the rotational motion is neglected in the approximate model (see also Figure S13). Thus, we see that reaction is promoted if the molecule is initially rotating and if it approaches the barrier with an appropriate rotational orientation and motion.

Inspection of how θ varies along the minimum energy path (MEP) for the TS and the high symmetry top, bridge, and hollow sites (Figure 3e) provides further insight about the observations regarding the rotational efficacy. On the way to the barrier, θ depends on the reaction coordinate in a clear nonmonotonic manner, especially for the top, TS, and bridge MEPs (which are also depicted in Figure 3f). The optimal θ value first decreases with the reaction coordinate, and then it sharply increases, after which it decreases again, before the molecule reaches the minimum barrier geometry (Figure 3e). For the initially nonrotating molecules, "steering" (i.e., the effect that the molecule is steered to the most favorable orientation for reaction by the forces acting on it[62]) cannot take place under these conditions because the molecule will "overshoot" its most favorable orientation once the most favorable value of θ starts changing in the opposite direction due to the angular momentum the molecule has acquired. Hence, steering, which can be especially effective for an initially nonrotating molecule,[62] will be counterproductive, and on a relative basis molecules with $J = 0$ will be nonreactive. Rather the opposite is observed: the faster the molecule is rotating initially, the higher the probability is that the molecule reacts (note that a larger fraction of the initial (θ, p_θ) phase space is reactive for $\nu = 0$, $J = 8$ than for $\nu = 0$, $J = 2$; see Figures 3c and 3b, respectively) and that it arrives at the barrier with an appropriate rotational phase (i.e., (θ, p_θ)) to react (see also Figure S14).

The reason HCl + Au(111) is characterized by such a large rotational efficacy, but the benchmark MMSR of H_2 + Cu(111) is not, becomes clear from the comparison of the anisotropy in the polar orientation in the region preceding the minimum TS in Figure 4. For reactive scattering H_2 from metal
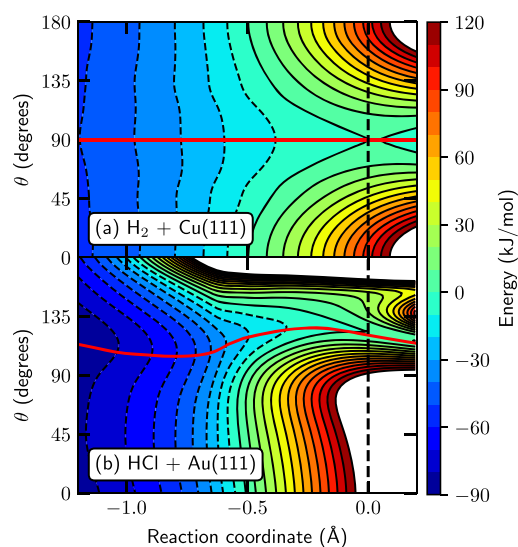
Figure 4. Two-dimensional cuts showing the PES at the minimum barrier geometries as a function of the reaction coordinate and the angle θ for H_2 + Cu(111) (panel a, as computed with the B86SRP68-vdW-DF2 DF[65]) and HCl + Au(111) (panel b, this work). Black contour lines are drawn at intervals of 10 kJ/mol between −90 and 120 kJ/mol, where the TS potential is taken as the zero; the dashed lines are for −90 to −10 kJ/mol, and the solid lines are for 0 to 120 kJ/mol. The red lines show the MEP, and the vertical black long dashed lines indicate the TSs.

surfaces, it is observed that rotation in states with low J hinders the reaction compared to $J = 0$ (i.e., "rotational hindering").[30,31,38−42,63,64] This observation is correlated to Figure 4a, which shows that the H_2 + Cu(111) PES should be effective at steering a molecule with $J = 0$ toward a favorable orientation for dissociation, as the preferred polar angle depends monotonically on the reaction coordinate in the region close to the barrier. Hence, for low J values, rotational pre-excitation of H_2 is ineffective since it hinders the steering. For HCl + Au(111) (Figure 4b), on the other hand, the PES is ineffective at steering, which agrees with earlier observation that the reaction of $J = 0$ HCl is inefficient. In fact, initial angular momentum now promotes the reaction as it allows for the molecule to be more easily focused toward the reactive channel (see Figure 3d and also Figure S6). The observed effect may be called a skewed rotational funnel effect, in analogy to the observation that when replenishing the oil in a car, the oil is best pointed at the far side of the skewed funnel that can be used for this purpose. We also note that the reactive channel of HCl on Au(111) (Figure 4b) is much more narrow than that of H_2 on Cu(111) (Figure 4a), which may also be important, but this was not analyzed further.

Our admittedly tentative explanation of the nonmonotonic dependence of the value of θ on the reaction path observed for most impact sites is as follows. We suspect that the initial bonding of the dissociating molecule to the surface goes via the more electronegative Cl atom; its increasingly attractive interaction with the surface and the initially mostly repulsive interaction of the H atom with the surface could explain why θ decreases initially with the reaction path coordinate in Figure 3e for all sites but the hollow site. For long enough distance between the H and Cl atoms, the H atom will also start bonding with the surface, which can explain the increase in the θ value of the reaction path starting at the value of roughly −0.6 Å of the reaction path coordinate in Figure 3e. We
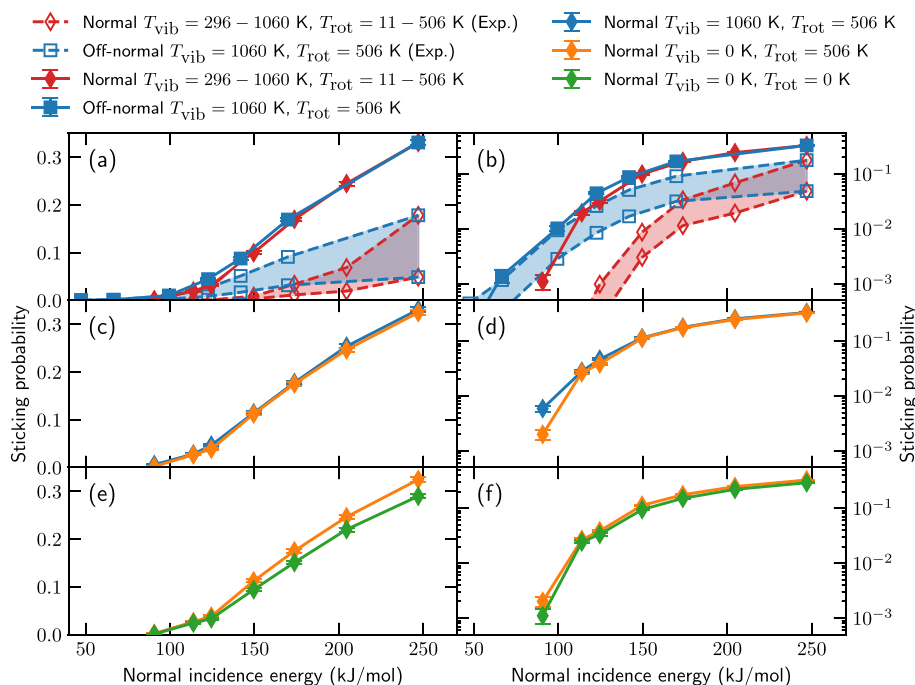
Figure 5. Sticking probability of HCl on Au(111) as a function of normal incidence energy for various conditions ((off-)normal incidence and vibrational and rotational temperatures). The open symbols and dashed lines indicate experimental results, where the shaded area indicates their uncertainty. The solid symbols and lines indicate computed results. The diamonds (squares) are for (off-)normal incidence, where the color indicates the rotational and vibrational temperatures (see legend). The error bars represent 68% confidence intervals. Panels b, d, and f are identical with panels a, c, and e, respectively, except that a logarithmic scale is used instead of a linear scale. For further explanation see the text.

suspect that the dissociation of hydrogen halides in general exhibits a similar reaction mechanism and that therefore experiments on hydrogen halides other than HCl might also yield a large rotational efficacy.

We now come back to the experiments that already exist for sticking of HCl on Au(111) and to what our calculations have to say about how energy partitioning in the incident HCl affected the sticking in these experiments. Figures 5a,b show that the agreement between theory (sold lines and filled symbols) and experiment (dashed lines and open symbols) is better for off-normal incidence (blue squares) than for normal incidence (red diamonds) of HCl. More importantly for the present paper, Figures 5c,d show that according to our theoretical results the sticking probability hardly depends on whether the incident molecules are vibrationally excited according to the highest nozzle temperature used ($T_{vib} = T_N = 1060$ K, blue diamonds) or not (0 K, orange diamonds). One reason for this is that even at the highest nozzle temperature only about 2% of the incident molecules are vibrationally excited. Furthermore, parallel translational energy does not influence the sticking probability (see also Figures S4g,h); that is, the NES approximation is valid. Finally, Figures 5e,f show that, in accordance with the high rotational efficacies predicted here, of all types of energy considered the rotational energy has the largest effect on the sticking. These figures give results for hypothetical normal incidence experiments with a rotational temperature of 0 K (green diamonds) and 506 K (the orange diamonds, 506 K is the maximum rotational temperature achieved in the experiments). In summary, the effect of rotational pre-excitation on the sticking of HCl is large, while the effect of initial vibrational pre-excitation is comparatively small. This invalidates an analysis of the experimental normal and off-normal incidence experiments in terms of dissociation

probabilities that only depend on the vibrational state population, as was previously used in ref 45 (see also section S3).

To summarize, in this work, a large effect of rotational pre-excitation is found for the dissociative chemisorption of HCl on Au(111). Surprisingly, rotational pre-excitation generally has a larger effect on the sticking probability than vibrational pre-excitation. The predicted rotational efficacy can be as large as a factor 20; that is, the rotational energy can be 20 times as effective at promoting the reaction as translational energy. To the best of our knowledge, a rotational efficacy this large, or even larger than one, has not been observed or predicted. Furthermore, pre-exciting both rotation and vibration has a mutually reinforcing effect: The rotational efficacy is increased considerably going from $\nu = 0$ to $\nu = 2$ (from a factor of about 4 to a factor 20). Moreover, the high rotational efficacy is not due to a steering effect, but to a skewed funnel effect where only specific initial rotational phases (i.e., combinations of the polar angle θ and its conjugate momentum) are reactive, which is caused by a nonmonotonic dependence of the reaction path on the polar angle θ in the region just in front of the minimum barrier. As a result, the reaction of HCl in the rotational ground state on Au(111) is hindered, whereas reaction of rotationally pre-excited HCl is promoted. We suspect that a similar rotational effect can be found for other hydrogen halides as well. Finally, the predicted rotational efficacy for HCl + Au(111) is strongly dependent on the employed DF and is therefore an important fingerprint of the accuracy of the DF for HCl + Au(111).

■ COMPUTATIONAL METHOD

In this work, the high-dimensional neural network potential (HDNNP) of ref 25 is employed. Here, a short summary of

the computational details for the density functional theory (DFT) calculations used to construct the HDNNP is given. A 3×3 Au(111) supercell with four layers and a 15 Å vacuum distance have been used. Furthermore, a plane wave kinetic energy cutoff of 600 eV and an $8 \times 8 \times 1$ Γ-centered k-point grid have been used. The top three layers have been relaxed in the Z direction, and the atoms in these layers are allowed to move to simulate a surface temperature of 170 K, in addition to a lattice expansion of 1.0014 due to the aforementioned surface temperature. All DFT calculations have been performed with a user modified version of the Vienna Ab-initio Simulation Package (VASP version 5.4.4)[66−70] to allow the use of the "made simple" revised Perdew, Burke, and Ernzerhof-like (MS-RPBEl) meta-GGA DF.[49] Sticking probabilities S_0 and initial-state selected reaction probabilities R were computed with the quasi-classical trajectory method.[71,72] The generation of the initial conditions and trajectory statistics of HCl are described in ref 44. Furthermore, the procedure to initialize the surface motion is described in ref 19.

■ ASSOCIATED CONTENT

ⓢ Supporting Information

The Supporting Information is available free of charge at https://pubs.acs.org/doi/10.1021/acs.jpclett.1c02093.

> Definition of the sticking probability (section S1), aspects of the computational methodology and of the associated accuracy (section S2), rovibrational efficacies obtained from effective barrier heights (section S3), description of an experimental procedure to obtain state-specific reaction probabilities (section S4), comparison of the two experimental data sets (section S5), further analysis of the mechanism underlying the high rotational efficacy (section S6), and a comparison between results obtained with the (R)PBE and MS-RPBEl DFs (section S7); experimental sticking probabilities of (off-)normal HCl and their error function fit (Figure S1), rovibrational state populations (Figure S2), predicted laser-on sticking probabilities for $\nu = 1$ (Figure S3), sticking probabilities while turning "computational knobs" when going from the conditions of one experimental data set to another (Figure S4), distribution of the θ angle during the reaction (Figures S5 and S6), sticking probability as a function of the initial θ angle (Figure S7), reactivity of initial θ and p_θ values for several rovibrational states as computed with MD (Figures S8−S10), generation of the initial orientation of HCl in the QCT approach (Figure S11), state-specific reactivity predicted by a simplistic model (Figures S12 and S13), θ angle along the reaction path for a few representative trajectories (Figure S14), anisotropy and corrugation of the PBE and MS-RPBEl PESs in the vicinity of a few site-specific barriers (Figures S15 and S16); parameters for error function fits to experimental sticking probabilities (Table S1), laser-on (Table S2) and state-specific (Table S3) sticking probabilities, and experimental beam parameters (Tables S4 and S5) (PDF)

■ AUTHOR INFORMATION

Corresponding Authors

Nick Gerrits − *Gorlaeus Laboratories, Leiden Institute of Chemistry, Leiden University, 2300 RA Leiden, The Netherlands;* ⓞ orcid.org/0000-0001-5405-7860; Email: n.gerrits@lic.leidenuniv.nl

Geert-Jan Kroes − *Gorlaeus Laboratories, Leiden Institute of Chemistry, Leiden University, 2300 RA Leiden, The Netherlands;* ⓞ orcid.org/0000-0002-4913-4689; Email: g.j.kroes@chem.leidenuniv.nl

Authors

Jan Geweke − *Department of Dynamics at Surfaces, Max Planck Institute for Biophysical Chemistry, 37077 Göttingen, Germany; Institute for Physical Chemistry, University of Göttingen, 37077 Göttingen, Germany;* ⓞ orcid.org/0000-0002-7743-1533

Daniel J. Auerbach − *Department of Dynamics at Surfaces, Max Planck Institute for Biophysical Chemistry, 37077 Göttingen, Germany*

Rainer D. Beck − *Laboratoire de Chimie Physique Moléculaire, École Polytechnique Fédérale de Lausanne, CH-1015 Lausanne, Switzerland;* ⓞ orcid.org/0000-0002-8152-8290

Complete contact information is available at:
https://pubs.acs.org/10.1021/acs.jpclett.1c02093

Notes

The authors declare no competing financial interest.

■ ACKNOWLEDGMENTS

■ REFERENCES

(1) Sorgenti, H. A.; Sachsel, G. F. Nitric Acid Manufacture—Theory and Practice. *Ind. Eng. Chem.* **1960**, *52*, 101−104.

(2) Ertl, G. Primary Steps in Catalytic Synthesis of Ammonia. *J. Vac. Sci. Technol., A* **1983**, *1*, 1247−1253.

(3) Rostrup-Nielsen, J. R.; Sehested, J.; Nørskov, J. K. *Advances in Catalysis*; Academic Press: 2002; Vol. 47, pp 65−139.

(4) Sá, S.; Silva, H.; Brandão, L.; Sousa, J. M.; Mendes, A. Catalysts for Methanol Steam Reforming—A Review. *Appl. Catal., B* **2010**, *99*, 43−57.

(5) Fisch, A. G. *Kirk-Othmer Encyclopedia of Chemical Technology*; John Wiley & Sons: 2019; pp 1−22.

(6) Wolcott, C. A.; Medford, A. J.; Studt, F.; Campbell, C. T. Degree of Rate Control Approach to Computational Catalyst Screening. *J. Catal.* **2015**, *330*, 197−207.

(7) Ertl, G. Elementary Steps in Heterogeneous Catalysis. *Angew. Chem., Int. Ed. Engl.* **1990**, *29*, 1219−1227.

(8) Sabbe, M. K.; Reyniers, M.-F.; Reuter, K. First-Principles Kinetic Modeling in Heterogeneous Catalysis: An Industrial Perspective on Best-Practice, Gaps and Needs. *Catal. Sci. Technol.* **2012**, *2*, 2010−2024.

(9) Juurlink, L. B. F.; McCabe, P. R.; Smith, R. R.; DiCologero, C. L.; Utz, A. L. Eigenstate-Resolved Studies of Gas-Surface Reactivity: CH₄ ν_3 Dissociation on Ni(100). *Phys. Rev. Lett.* **1999**, *83*, 868−871.

(10) Smith, R. R.; Killelea, D. R.; DelSesto, D. F.; Utz, A. L. Preference for Vibrational over Translational Energy in a Gas-Surface Reaction. *Science* **2004**, *304*, 992−995.

(11) Killelea, D. R.; Campbell, V. L.; Shuman, N. S.; Utz, A. L. Bond-Selective Control of a Heterogeneously Catalyzed Reaction. *Science* **2008**, *319*, 790−793.

(12) Juurlink, L. B. F.; Killelea, D. R.; Utz, A. L. State-Resolved Probes of Methane Dissociation Dynamics. *Prog. Surf. Sci.* **2009**, *84*, 69−134.

(13) Shen, X. J.; Lozano, A.; Dong, W.; Busnengo, H. F.; Yan, X. H. Towards Bond Selective Chemistry from First Principles: Methane on Metal Surfaces. *Phys. Rev. Lett.* **2014**, *112*, 046101.

(14) Hundt, P. M.; Ueta, H.; van Reijzen, M. E.; Jiang, B.; Guo, H.; Beck, R. D. Bond-Selective and Mode-Specific Dissociation of CH_3D and CH_2D_2 on Pt(111). *J. Phys. Chem. A* **2015**, *119*, 12442−12448.

(15) Jiang, B.; Guo, H. Dynamics of Water Dissociative Chemisorption on Ni(111): Effects of Impact Sites and Incident Angles. *Phys. Rev. Lett.* **2015**, *114*, 166101.

(16) Zhang, Z.; Liu, T.; Fu, B.; Yang, X.; Zhang, D. H. First-Principles Quantum Dynamical Theory for the Dissociative Chemisorption of H_2O on Rigid Cu(111). *Nat. Commun.* **2016**, *7*, 11953.

(17) Nattino, F.; Migliorini, D.; Kroes, G.-J.; Dombrowski, E.; High, E. A.; Killelea, D. R.; Utz, A. L. Chemically Accurate Simulation of a Polyatomic Molecule-Metal Surface Reaction. *J. Phys. Chem. Lett.* **2016**, *7*, 2402−2406.

(18) Migliorini, D.; Chadwick, H.; Nattino, F.; Gutiérrez-González, A.; Dombrowski, E.; High, E. A.; Guo, H.; Utz, A. L.; Jackson, B.; Beck, R. D.; et al. Surface Reaction Barriometry: Methane Dissociation on Flat and Stepped Transition-Metal Surfaces. *J. Phys. Chem. Lett.* **2017**, *8*, 4177−4182.

(19) Gerrits, N.; Migliorini, D.; Kroes, G.-J. Dissociation of CHD_3 on Cu(111), Cu(211), and Single Atom Alloys of Cu(111). *J. Chem. Phys.* **2018**, *149*, 224701.

(20) Chadwick, H.; Migliorini, D.; Kroes, G. J. CHD_3 Dissociation on Pt(111): A Comparison of the Reaction Dynamics Based on the PBE Functional and on a Specific Reaction Parameter Functional. *J. Chem. Phys.* **2018**, *149*, 044701.

(21) Gerrits, N.; Kroes, G.-J. An AIMD Study of Dissociative Chemisorption of Methanol on Cu(111) with Implications for Formaldehyde Formation. *J. Chem. Phys.* **2019**, *150*, 024706.

(22) Gerrits, N.; Shakouri, K.; Behler, J.; Kroes, G.-J. Accurate Probabilities for Highly Activated Reaction of Polyatomic Molecules on Surfaces Using a High-Dimensional Neural Network Potential: CHD_3 + Cu(111). *J. Phys. Chem. Lett.* **2019**, *10*, 1763−1768.

(23) Gerrits, N.; Chadwick, H.; Kroes, G.-J. Dynamical Study of the Dissociative Chemisorption of CHD_3 on Pd(111). *J. Phys. Chem. C* **2019**, *123*, 24013−24023.

(24) Gerrits, N.; Kroes, G.-J. Curious Mechanism of the Dissociative Chemisorption of Ammonia on Ru(0001). *J. Phys. Chem. C* **2019**, *123*, 28291−28300.

(25) Gerrits, N.; Geweke, J.; Smeets, E. W. F.; Voss, J.; Wodtke, A. M.; Kroes, G.-J. Closing the Gap Between Experiment and Theory: Reactive Scattering of HCl from Au(111). *J. Phys. Chem. C* **2020**, *124*, 15944−15960.

(26) Moiraghi, R.; Lozano, A.; Peterson, E.; Utz, A.; Dong, W.; Busnengo, H. F. Nonthermalized Precursor-Mediated Dissociative Chemisorption at High Catalysis Temperatures. *J. Phys. Chem. Lett.* **2020**, *11*, 2211−2218.

(27) Jackson, B. Direct and Trapping-Mediated Pathways to Dissociative Chemisorption: CH_4 Dissociation on Ir(111) with Step Defects. *J. Chem. Phys.* **2020**, *153*, 034704.

(28) Zeng, X.; Qiu, Z.; Li, P.; Li, Z.; Yang, J. Steric Hindrance Effect in High-Temperature Reactions. *CCS Chem.* **2020**, *2*, 460−467.

(29) Rettner, C. T.; DeLouise, L. A.; Auerbach, D. J. Effect of Incidence Kinetic Energy and Surface Coverage on the Dissociative Chemisorption of Oxygen on W(110). *J. Chem. Phys.* **1986**, *85*, 1131−1149.

(30) Michelsen, H. A.; Rettner, C. T.; Auerbach, D. J.; Zare, R. N. Effect of Rotation on the Translational and Vibrational Energy Dependence of the Dissociative Adsorption of D_2 on Cu(111). *J. Chem. Phys.* **1993**, *98*, 8294−8307.

(31) Rettner, C. T.; Michelsen, H. A.; Auerbach, D. J. Quantum-state-specific Dynamics of the Dissociative Adsorption and Associative Desorption of H_2 at a Cu(111) Surface. *J. Chem. Phys.* **1995**, *102*, 4625−4641.

(32) Luntz, A. C.; Brown, J. K.; Williams, M. D. Molecular Beam Studies of H_2 and D_2 Dissociative Chemisorption on Pt(111). *J. Chem. Phys.* **1990**, *93*, 5240−5246.

(33) Chadwick, H.; Guo, H.; Gutiérrez-González, A.; Menzel, J. P.; Jackson, B.; Beck, R. D. Methane Dissociation on the Steps and Terraces of Pt(211) Resolved by Quantum State and Impact Site. *J. Chem. Phys.* **2018**, *148*, 014701.

(34) Migliorini, D.; Nattino, F.; Tiwari, A. K.; Kroes, G.-J. HOD on Ni(111): Ab Initio Molecular Dynamics Prediction of Molecular Beam Experiments. *J. Chem. Phys.* **2018**, *149*, 244706.

(35) Chen, J.; Zhou, X.; Zhang, Y.; Jiang, B. Vibrational Control of Selective Bond Cleavage in Dissociative Chemisorption of Methanol on Cu(111). *Nat. Commun.* **2018**, *9*, 4039.

(36) Díaz, C.; Olsen, R. A.; Auerbach, D. J.; Kroes, G. J. Six-Dimensional Dynamics Study of Reactive and Non Reactive Scattering of H_2 from Cu(111) Using a Chemically Accurate Potential Energy Surface. *Phys. Chem. Chem. Phys.* **2010**, *12*, 6499−6519.

(37) Donald, S. B.; Harrison, I. Rice−Ramsperger−Kassel−Marcus Simulation of Hydrogen Dissociation on Cu(111): Addressing Dynamical Biases, Surface Temperature, and Tunneling. *J. Phys. Chem. C* **2014**, *118*, 320−337.

(38) Xiao, Y.; Dong, W.; Busnengo, H. F. Reactive Force Fields for Surface Chemical Reactions: A Case Study with Hydrogen Dissociation on Pd Surfaces. *J. Chem. Phys.* **2010**, *132*, 014704.

(39) Chen, J.-C.; Ramos, M.; Arasa, C.; Juanes-Marcos, J. C.; Somers, M. F.; Martinez, A. E.; Diaz, C.; Olsen, R. A.; Kroes, G.-J. Dynamics of H_2 Dissociation on the 1/2 ML c(2 × 2)-Ti/Al(100) Surface. *Phys. Chem. Chem. Phys.* **2012**, *14*, 3234−3247.

(40) Wijzenbroek, M.; Helstone, D.; Meyer, J.; Kroes, G.-J. Dynamics of H_2 Dissociation on the Close-Packed (111) Surface of the Noblest Metal: H_2 + Au(111). *J. Chem. Phys.* **2016**, *145*, 144701.

(41) Shuai, Q.; Kaufmann, S.; Auerbach, D. J.; Schwarzer, D.; Wodtke, A. M. Evidence for Electron−Hole Pair Excitation in the Associative Desorption of H_2 and D_2 from Au(111). *J. Phys. Chem. Lett.* **2017**, *8*, 1657−1663.

(42) Kaufmann, S.; Shuai, Q.; Auerbach, D. J.; Schwarzer, D.; Wodtke, A. M. Associative Desorption of Hydrogen Isotopologues from Copper Surfaces: Characterization of Two Reaction Mechanisms. *J. Chem. Phys.* **2018**, *148*, 194703.

(43) Juurlink, L. B.; Smith, R. R.; Utz, A. L. The Role of Rotational Excitation in the Activated Dissociative Chemisorption of Vibrationally Excited Methane on Ni(100). *Faraday Discuss.* **2000**, *117*, 147−160.

(44) Füchsel, G.; del Cueto, M.; Díaz, C.; Kroes, G.-J. Enigmatic HCl + Au(111) Reaction: A Puzzle for Theory and Experiment. *J. Phys. Chem. C* **2016**, *120*, 25760−25779.

(45) Shirhatti, P. R.; Geweke, J.; Steinsiek, C.; Bartels, C.; Rahinov, I.; Auerbach, D. J.; Wodtke, A. M. Activated Dissociation of HCl on Au(111). *J. Phys. Chem. Lett.* **2016**, *7*, 1346−1350.

(46) Liu, T.; Fu, B.; Zhang, D. H. Six-Dimensional Quantum Dynamics Study for the Dissociative Adsorption of HCl on Au(111) Surface. *J. Chem. Phys.* **2013**, *139*, 184705.

(47) Liu, Q.; Zhou, X.; Zhou, L.; Zhang, Y.; Luo, X.; Guo, H.; Jiang, B. Constructing High-Dimensional Neural Network Potential Energy Surfaces for Gas−Surface Scattering and Reactions. *J. Phys. Chem. C* **2018**, *122*, 1761−1769.

(48) Füchsel, G.; Zhou, X.; Jiang, B.; Juaristi, J. I.; Alducin, M.; Guo, H.; Kroes, G.-J. Reactive and Nonreactive Scattering of HCl from Au(111): An Ab Initio Molecular Dynamics Study. *J. Phys. Chem. C* **2019**, *123*, 2287−2299.

(49) Smeets, E. W.; Voss, J.; Kroes, G.-J. Specific Reaction Parameter Density Functional Based on the Meta-Generalized Gradient Approximation: Application to H_2 + Cu(111) and H_2 + Ag(111). *J. Phys. Chem. A* **2019**, *123*, 5395−5406.

(50) Gerrits, N.; Smeets, E. W. F.; Vuckovic, S.; Powell, A. D.; Doblhoff-Dier, K.; Kroes, G.-J. Density Functional Theory for

Molecule−Metal Surface Reactions: When Does the Generalized Gradient Approximation Get It Right, and What to Do If It Does Not. *J. Phys. Chem. Lett.* **2020**, *11*, 10552−10560.

(51) Liu, T.; Fu, B.; Zhang, D. H. HCl Dissociating on a Rigid Au(111) Surface: A Six-Dimensional Quantum Mechanical Study on a New Potential Energy Surface Based on the RPBE Functional. *J. Chem. Phys.* **2017**, *146*, 164706.

(52) Rahinov, I.; Cooper, R.; Yuan, C.; Yang, X.; Auerbach, D. J.; Wodtke, A. M. Efficient Vibrational and Translational Excitations of a Solid Metal Surface: State-to-State Time-of-Flight Measurements of HCl(ν = 2,J = 1) Scattering from Au(111). *J. Chem. Phys.* **2008**, *129*, 214708.

(53) Geweke, J.; Shirhatti, P. R.; Rahinov, I.; Bartels, C.; Wodtke, A. M. Vibrational Energy Transfer near a Dissociative Adsorption Transition State: State-to-State Study of HCl Collisions at Au(111). *J. Chem. Phys.* **2016**, *145*, 054709.

(54) Whitehead, J. C. Plasma−Catalysis: The Known Knowns, the Known Unknowns and the Unknown Unknowns. *J. Phys. D: Appl. Phys.* **2016**, *49*, 243001.

(55) Mehta, P.; Barboun, P.; Go, D. B.; Hicks, J. C.; Schneider, W. F. Catalysis Enabled by Plasma Activation of Strong Chemical Bonds: A Review. *ACS Energy Lett.* **2019**, *4*, 1115−1133.

(56) Bogaerts, A.; Tu, X.; Whitehead, J. C.; Centi, G.; Lefferts, L.; Guaitella, O.; Azzolina-Jury, F.; Kim, H.-H.; Murphy, A. B.; Schneider, W. F.; et al. The 2020 Plasma Catalysis Roadmap. *J. Phys. D: Appl. Phys.* **2020**, *53*, 443001.

(57) Neyts, E. C.; Ostrikov, K. K.; Sunkara, M. K.; Bogaerts, A. Plasma Catalysis: Synergistic Effects at the Nanoscale. *Chem. Rev.* **2015**, *115*, 13408−13446.

(58) Hong, J.; Pancheshnyi, S.; Tam, E.; Lowke, J. J.; Prawer, S.; Murphy, A. B. Kinetic Modelling of NH_3 Production in N_2-H_2 Non-Equilibrium Atmospheric-Pressure Plasma Catalysis. *J. Phys. D: Appl. Phys.* **2017**, *50*, 154005.

(59) Ma, H.; Schneider, W. F. Structure- and Temperature-Dependence of Pt-Catalyzed Ammonia Oxidation Rates and Selectivities. *ACS Catal.* **2019**, *9*, 2407−2414.

(60) Michiels, R.; Engelmann, Y.; Bogaerts, A. Plasma Catalysis for CO_2 Hydrogenation: Unlocking New Pathways toward CH_3OH. *J. Phys. Chem. C* **2020**, *124*, 25859−25872.

(61) Engelmann, Y.; Mehta, P.; Neyts, E. C.; Schneider, W. F.; Bogaerts, A. Predicted Influence of Plasma Activation on Non-Oxidative Coupling of Methane on Transition Metal Catalysts. *ACS Sustainable Chem. Eng.* **2020**, *8*, 6043−6054.

(62) Gross, A.; Wilke, S.; Scheffler, M. Six-Dimensional Quantum Dynamics of Adsorption and Desorption of H_2 at Pd(100): Steering and Steric Effects. *Phys. Rev. Lett.* **1995**, *75*, 2718−2721.

(63) Somers, M. F.; McCormack, D. A.; Kroes, G. J.; Olsen, R. A.; Baerends, E. J.; Mowrey, R. C. Signatures of Site-Specific Reaction of H_2 on Cu(100). *J. Chem. Phys.* **2002**, *117*, 6673−6687.

(64) Kroes, G.-J.; Somers, M. F. Six-Dimensional Dynamics of Dissociative Chemisorption of H_2 on Metal Surfaces. *J. Theor. Comput. Chem.* **2005**, *04*, 493−581.

(65) Smeets, E. W. F.; Kroes, G.-J. Designing New SRP Density Functionals Including Non-Local vdW-DF2 Correlation for H_2 + Cu(111) and Their Transferability to H_2 + Ag(111), Au(111) and Pt(111). *Phys. Chem. Chem. Phys.* **2021**, *23*, 7875−7901.

(66) Kresse, G.; Hafner, J. Ab Initio Molecular-Dynamics Simulation of the Liquid-Metal−Amorphous-Semiconductor Transition in Germanium. *Phys. Rev. B: Condens. Matter Mater. Phys.* **1994**, *49*, 14251−14269.

(67) Kresse, G.; Hafner, J. Ab Initio Molecular Dynamics for Liquid Metals. *Phys. Rev. B: Condens. Matter Mater. Phys.* **1993**, *47*, 558−561.

(68) Kresse, G.; Furthmüller, J. Efficient Iterative Schemes for Ab Initio Total-Energy Calculations Using a Plane-Wave Basis Set. *Phys. Rev. B: Condens. Matter Mater. Phys.* **1996**, *54*, 11169−11186.

(69) Kresse, G.; Furthmüller, J. Efficiency of Ab-Initio Total Energy Calculations for Metals and Semiconductors Using a Plane-Wave Basis Set. *Comput. Mater. Sci.* **1996**, *6*, 15−50.

(70) Kresse, G.; Joubert, D. From Ultrasoft Pseudopotentials to the Projector Augmented-Wave Method. *Phys. Rev. B: Condens. Matter Mater. Phys.* **1999**, *59*, 1758−1775.

(71) Karplus, M.; Porter, R. N.; Sharma, R. D. Exchange Reactions with Activation Energy. I. Simple Barrier Potential for (H, H_2). *J. Chem. Phys.* **1965**, *43*, 3259−3287.

(72) Porter, R. N.; Raff, L. M. In *Dynamics of Molecular Collisions: Part B*; Miller, W. H., Ed.; Modern Theoretical Chemistry; Springer: Boston, MA, 1976; pp 1−52.